Electronic Supplementary Material (ESI) for Materials Horizons.
This journal is © The Royal Society of Chemistry 2022

Resistance-switchable conjugated polyrotaxane for flexible high-performance RRAMs

Jiankui Zhou,[a] Hanfang Feng,[a] Qingqing Sun,[a] Zhengkun Xie,[b] Xinchang Pang,[a] Takeo Minari,[c] Xuying Liu,*[a] and Li Zhang*[a]*

1 Experimental Procedures

1.1 Materials

Aniline (A.R.) was purchased from Sinopharm Chemical Reagent Co. Ltd. in China, and purified by distillation before use. β-cyclodextrin (CD, A.R.), ammonium persulfate (APS, A.R.), N-methyl-2-pyrrolidone (NMP, 99%), dimethyl sulfoxide (DMSO, 99%), N,N-dimethylformamide (DMF,99%), ethanol (95%), concentrated hydrochloric acid (HCl, 36.0 38.0%) and ammonium hydroxide ($NH_3 \cdot H_2O$, 25.0 28.0%), Mercury (Hg, A.R.) were from Sinopharm Chemical Reagent Co. Ltd. and used as received. (Methyl sulfoxide)-d_6 (DMSO-d_6, 99.8%) was bought from J&K Scientific Ltd. ITO glasses (20 $\Omega \cdot sq^{-1}$) was provided by Advanced Election Technology Co. Ltd. Gold (Au, 99%) and aluminum (Al, 99.999%) were obtained from Xi'an Polymer Light Technology Corp. in China.

1.2 Synthesis of conjugated polyrotaxane (CPR1)

For the synthesis of CPR1, freshly distilled aniline (93 mg, 1.0 mmol) was added into a 50 mL aqueous solution of β-cyclodextrin (1.135 g, 1.0 mmol), followed by stirring at 0 °C for 4 h until a clear solution was obtained. After that, the concentrated HCl (5 mL) and APS (228 mg, 1.0 mmol) were successively added with further stirring at 0 °C for 12 h. The precipitate was collected by filtration, washed with ice water and ethanol, and freeze-dried for 10h to produce CPR1 (379 mg, yield 31%) as a dark blue powder. Elemental analysis for $C_{42}H_{70}O_{35} \bullet 1.6C_6H_4N$ was carried out with element contents shown in Table S1. For comparison, some reference samples were also prepared. Doped polyaniline (dPAN) was obtained via the same preparation procedure in the absence of CD, which was treated with excess $NH_3 \cdot H_2O$ solution for 12 h to yield intrinsic polyaniline (iPAN).

1.3 Fabrication of CPR1 RRAM device

The ITO glasses (2×2 cm^2) were ultrasonically cleaned by using acetone, ethanol and deionized water successively. After drying via nitrogen gas flow, the ITO glasses were exposed to oxygen plasma treatment for 20 min. CPR1 was dissolved in deionized water (5 mg/mL) under stirring at 0°C, followed by spin coating onto the precleaned ITO glass at a spinning speed of 2000 rpm for 30 s. Subsequently, the CPR1 film was dried at room temperature for 5min and then annealed at 80 °C in vacuum for 10 h. The thickness of the CPR1 film was determined by using a profilometer (model DektakXT, Bruker). Finally, the Al (or Au) top electrode of 150 nm was thermally evaporated using a shadow mask to form a circular pattern with diameters of 100, 200, and 300 μm. For Au/CPR1/Au symmetric device, the crossbar configuration was utilized. According to the above procedure, the reference devices employing pure CD, iPAN, dPAN, as well as the simple mixture of CD and iPAN as the respective active layer were also fabricated by using NMP as alternative solvent. Especially, for the simple mixture CD-iPAN device, 157 mg of CD and 20 mg of iPAN (calculated on 1.6 phenyl units of iPAN per CD molecule) were mixed in the NMP solvent (30 mL) and then used for spin-coating. For the in-site spectroscopic analysis of RRAM device, the liquid mercury tiny droplet was applied as top electrode, which is able to be removed from the CPR1 film after the voltage application.

1.4 Fabrication of fully-printed Au/CPR1/Au/PEN device arrays

The large-scale device arrays were fabricated by layer-by-layer printing of bottom Au electrode, CPR1 active layer and top Au electrode as reported previously. 125-μm-thick PEN film with the surface modification layer of parylene-C (1.5 μm) was used as the substrate. The bottom electrode was fabricated based on the application of water-based AuNP ink onto the parylene-C surface patterned with different wettability. The hydrophobic/hydrophilic areas were defined by the vacuum ultraviolet (VUV) light treatment (wave length of 172 nm) through a photomask for 100 s, which rendered the hydrophobic parylene-C surface into hydrophilic. Then,

the water-based AuNP ink (25 wt%) was printed by a coating bar to form patterned Au electrodes on the hydrophilic areas with the drying process at room temperature. Following that, the guide layer was constructed through screen printing using the Cytop solution (Asahi Glass Co. Ltd), which formed blank arrays in the electrode regions with a depth of 1 μm for the selective deposition of active layers. The CPR1 ink (5 mg/mL) was drop-casted on the blank area, followed by annealing at 80^{o}C in vacuum for 10 h. Subsequently, the top Au electrode was printed by drop casting AuNP ink on the blank area as well with drying at room temperature. Finally, the Cytop layer was washed away to fabricate the flexible and patterned RRAM device arrays.

1.5 Characterization

UV-vis absorption spectra were recorded on a UV-2401PC UV-vis recording spectrophotometer (Shimadzu, Japan). Fourier transform infrared spectra (FTIR) including transmission mode and attenuated total reflectance (ATR) mode were performed on A TENSOR-II FT-IR spectrometer (Bruker). ^{1}H-NMR spectra were recorded on a DPX-400 MHz NMR spectrometer (Bruker) by using DMSO-d6 as solvent. The X-ray diffraction (XRD) patterns were analyzed from an X-Ray diffractometer (Rigaku, RINT-2500) with a Cu Kα radiation source (λ=1.542 Å), and the XRD data were recorded at room temperature in the range of 5-60° with a step size of 0.02° and at a scanning speed of 2° min^{-1}. Elemental analyses were carried out on a Perkin-Elmer 2400C instrument. Atomic force microscopic (AFM) images were taken from Nanoscope III MultiMode SPM (Digital Instruments) with an AS-12 ("E") scanner operated in tapping mode in conjunction with a V-shaped tapping tip. The AFM samples were prepared by spin-coating the sample solution on the freshly cleaved mica or precleaned ITO glass and then dried naturally at room temperature over 24h. The cross-sectional SEM images were performed on a field emission scanning electron microscope (FESEM) (JSM-7001F) with the electron beam accelerated at 10 kV. X-ray photoelectron spectroscopy (XPS) was applied on an ESCALAB 250 photoelectron spectrometer (ThermoFisher Scientific) with Al Kα (1486.6 eV) as the X-ray source set at 150 W and a pass energy of 30 eV for high-resolution scanning. RS characteristics of unsealed RRAM devices were measured on a home-made probe station equipped with a temperature controller in an ambient environment, where the different humidity level was obtained by introducing a mixed gas flow of dry and wet gases. The probe station was connected to a semiconductor analyzer (Agilent B1500A) working in either voltage sweeping mode or voltage pulse mode. For the *I-V* characteristic of the all-printed flexible device, the PEN substrate were fixed between the jaws of the adjustable and readable vernier calipers. The different curvature radius of the bending device was realized by adjusting the distance between the jaws. The memory cells at the top middle of the ridge of the bended substrate was tested at different curvature radius and the curvature radius of 3 mm is the limit of this method. The bending endurance was implemented by bending the device to the curvature radius of 3 mm and recovering to flat for 1000 cycles with the same test to the cell.

2 Results and Discussion

2.1 Structure characterization of CPR1

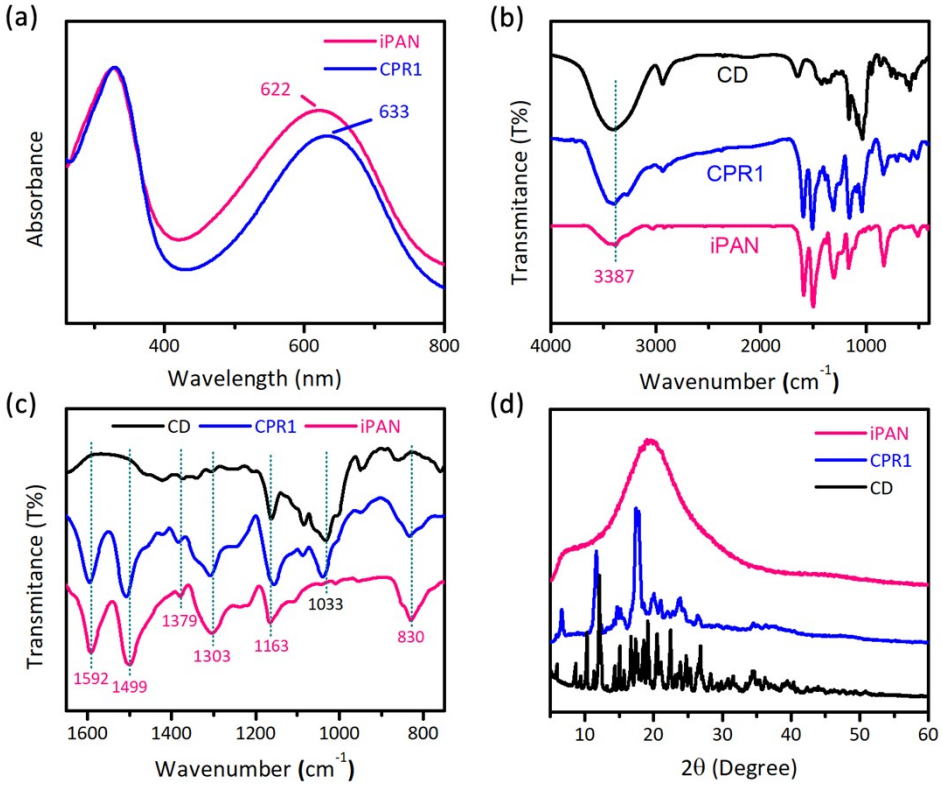

Fig. S1 (a) UV–vis spectra of CPR1 and iPAN in NMP. FTIR spectra in (b) 450~4000cm^{-1} and (c) 750~1650cm^{-1}, and (d) XRD spectra of CPR1, native CD, and free iPAN.

UV-vis spectra of CPR1 and free iPAN (obtained by dedoping from dPAN) were recorded in NMP solutionwith the result illustrated in Fig. S1a. It is seen that the n-π* transition band of CPR1 is red-shifted by 10 nm with respect to free iPAN, concurrent with the decrease of band intensity, suggesting that the iPAN chain in CPR1 has a better coplanar characteristic due to the confinement effect of CD inclusion.[1] The chemical structure of CPR1 were further investigated by FTIR and XRD measurements with free iPAN and native CD as comparison. In Fig. S1b and Fig. S1c, the FTIR spectrum of CPR1 is nearly the superposition of those of free iPAN and native CD except some band shifts. The stretching vibration bands of iPAN assigned to N-H, quinoid, benzenoid, imine C-N and amine C-N occur at 3387, 1592, 1499, 1379 and 1303 cm^{-1} respectively. These bands as well as the CD stretching band at 1033 cm^{-1} (C-O-C) appear blue-shifted in the spectrum of CPR1, indicating that iPAN was successfully included in the cavity of CD.[2, 3] At the same time, the CD band at 1160 cm^{-1} (C-O stretching in C-OH) is red-shifted and intensified in the spectrum of CPR1, implying the formation of intercomponent H-bonding between iPAN and CD.[4] Moreover, after encapsulation, the aromatic C-H in-plane deformation of iPAN at 1163 cm^{-1} shifts to lower frequency and the out-of-plane band at 830 cm^{-1} shifts reversely, revealing the coplanar and conjugated feature of iPAN in CD, which is in accordance with the result of UV-vis spectra. According to the XRD patters in Fig. S1d, the native CD forms a cage-type crystal structure,[5] and the free iPAN has an amorphous character. Differently, the two major diffraction peaks at 11.6 and 17.5 were observed for CPR1, which have been known to be the characteristic diffraction peaks of a channel-type structure of CD,[6] implying that the CD rings are rearranged one by one and threaded on the iPAN chain in the product.

Table S1 The elemental analysis of CPR1

$C_{42}H_{70}O_{35}\cdot1.6C_6H_4N$	C	H	N
Calcd.	48.44	6.03	1.75
Found	48.39	5.97	1.82

2.2 The solubility performance of CPR1

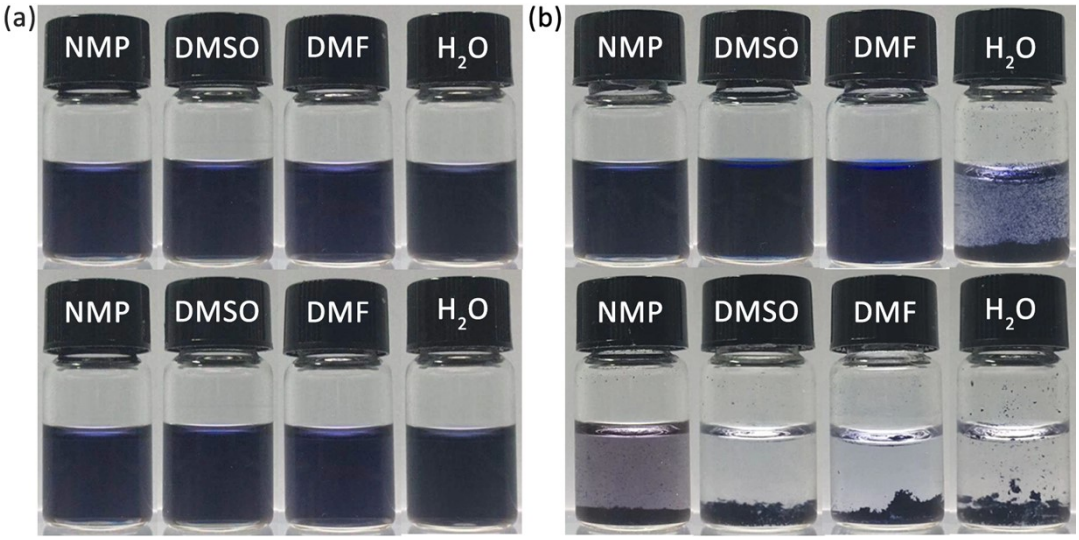

Fig. S2 The digital photos of equivalent (a) CPR1 (5 mg/mL) and (b) iPAN (0.6 mg/mL) solutions in different polar solvents before (top row) and after (bottom row) two-month standing.

The solubility performance shows that CPR1 is readily soluble in water, NMP, DMF and DMSO at higher concentration (5 mg/mL) and remains stably soluble for more than two months, while free iPAN of equivalent amount (0.6 mg/mL) is poorly to moderately soluble in these solvents, and displays the obvious sedimentation after two-month standing. This enhanced solubility of CPR1, especially in water, may provide a facile and green processability for the potential applications of PAN in a variety of electronic devices.

2.3 The surface morphology of CPR1 film on the ITO substrate

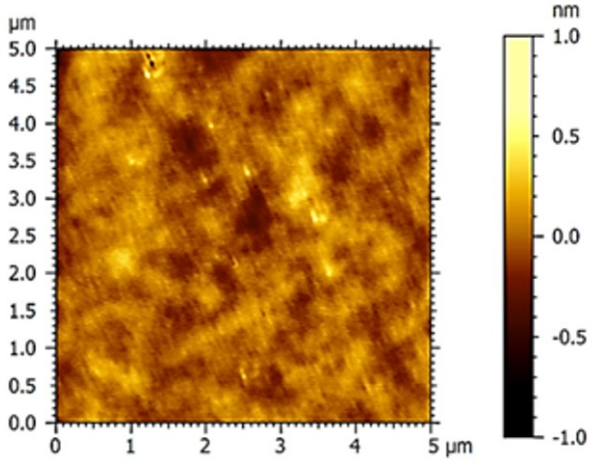

Fig. S3 Topological AFM image of CPR1 film prepared by spin-coating the aqueous solution of CPR1 (5 mg/mL) on the ITO substrate.

Table S2 The cycle-to-cycle uniformity analysis of switching parameters.

(a) Calculated Δ, μ and Δ/μ values for the present Al/CPR1/ITO device.

	R_{LRS}	R_{HRS}	V_{set}	V_{reset}
σ	48.3 Ω	511.4 MΩ	-1.347 V	1.581 V
μ	4.8 Ω	185.1 MΩ	0.033 V	0.051 V
$\lvert\Delta/\mu\rvert$	0.0990	0.3620	0.0247	0.0324

(b) The uniformity comparison of the present Al/CPR1/ITO device with other RRAM devices.

Device	**$\lvert\Delta/\mu\rvert$**				**Ref.**
	R_{LRS}	R_{HRS}	V_{set}	V_{reset}	
Al/CPR1/ITO	**0.0990**	**0.3620**	**0.0247**	**0.0324**	**This work**
Al/glucose/p^+Si	-	-	0.0630	0.1033	7
TiN/HfO_x/Pt/Ti/SiO_2	0.0250	0.0940	-	-	8
Ta/Ta_2O_5/Pt	0.2500	0.2900	0.1400	0.0550	9
Pt/PA-TsOH/Pt	0.0391	0.0966	0.0255	0.0231	10
Al/Ge/TaO_x/Pt	0.2100	1.3300	0.3980	0.2314	11

The cycle-to-cycle uniformity of switching parameters (R_{LRS}, R_{HRS}, V_{set} and V_{reset}) is evaluated by the standard deviation (Δ) to mean (μ) ratio. As shown in Table S2a, our CPR1 device features the Δ/μ values of 0.0990, 0.3620, 0.0247 and 0.0324, respectively, for the device resistance in LRS and HRS and the corresponding SET and RESET voltages. Table S2b compares the Δ/μ values of the present Al/CPR1/ITO with other reported RRAM devices. It is found that the present Al/CPR1/ITO device exhibits the lower Δ/μ values compared to most of other RRAM devices, suggesting its excellent uniformity in the device performance.

2.4 Environmental stability of CPR1 RRAM device

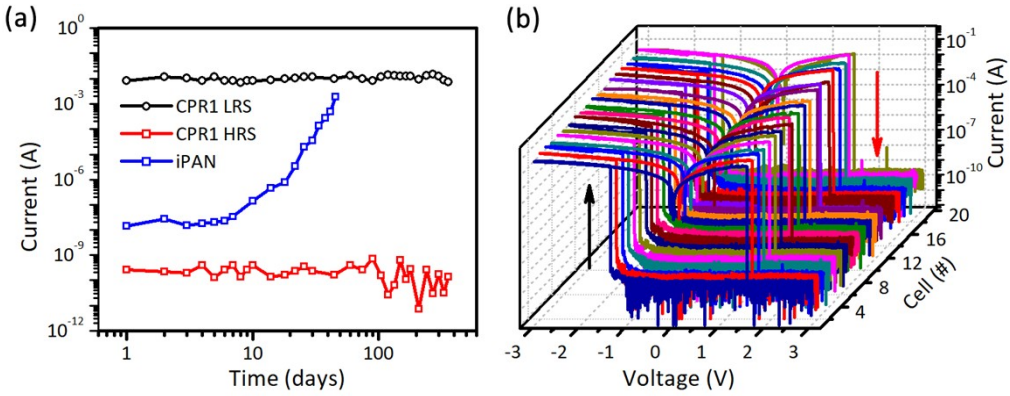

Fig. S4 (a) Long-term data retention measurements of Al/CPR1/ITO device by intermittently monitoring the HRS or LRS using the read voltage of 0.1V during device storage under ambient conditions, and the current evolution with time for reference Al/iPAN/ITO device. The thickness of active layer is 150 nm and the diameter of top electrode is 100 μm. (b) The I-V characteristics of 20 cells for Al/CPR1/ITO device after 1 year of storage under ambient environment.

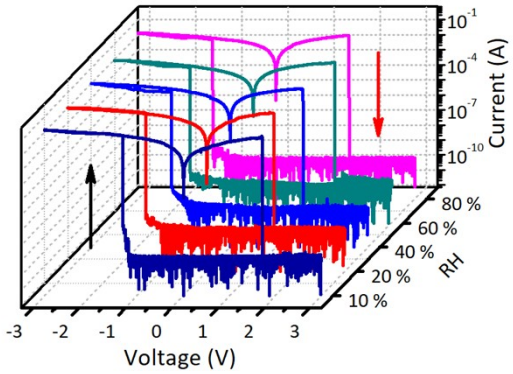

Fig. S5 I-V characteristics of Al/CPR1/ITO device under various relative humidity.

2.5 Measurements on CPR1 RRAM device for supporting the RS mechanism

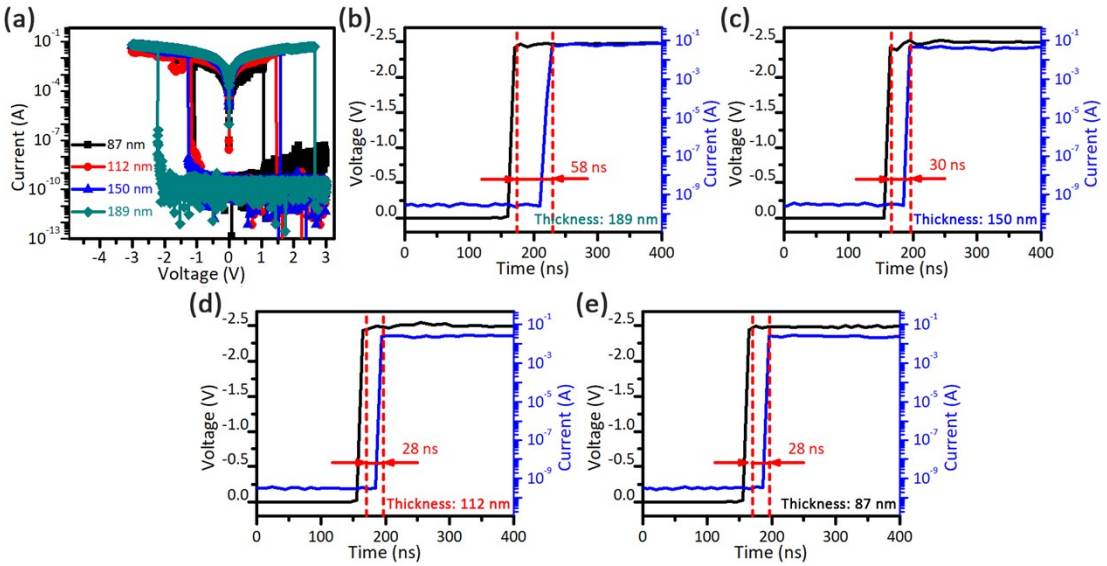

Fig. S6 (a) The I-V behaviors and (b-e) switching speed test of Al/CPR1/ITO devices with varied film thicknesses.

Fig. S6 depicts the memory performances and switching speed tests with respect to the active layer thickness of Al/CPR1/ITO device. These devices exhibit typical bipolar RS performance as shown in Fig. S6a. The operation voltage of the device with thinner thickness is lower, while the device with thicker thickness needs larger voltage to be turned on. Nevertheless, all these devices reveal the fast switching speed (28 ~58ns) regardless of their active layer thickness (87 189 nm) (Fig. S6b-e).

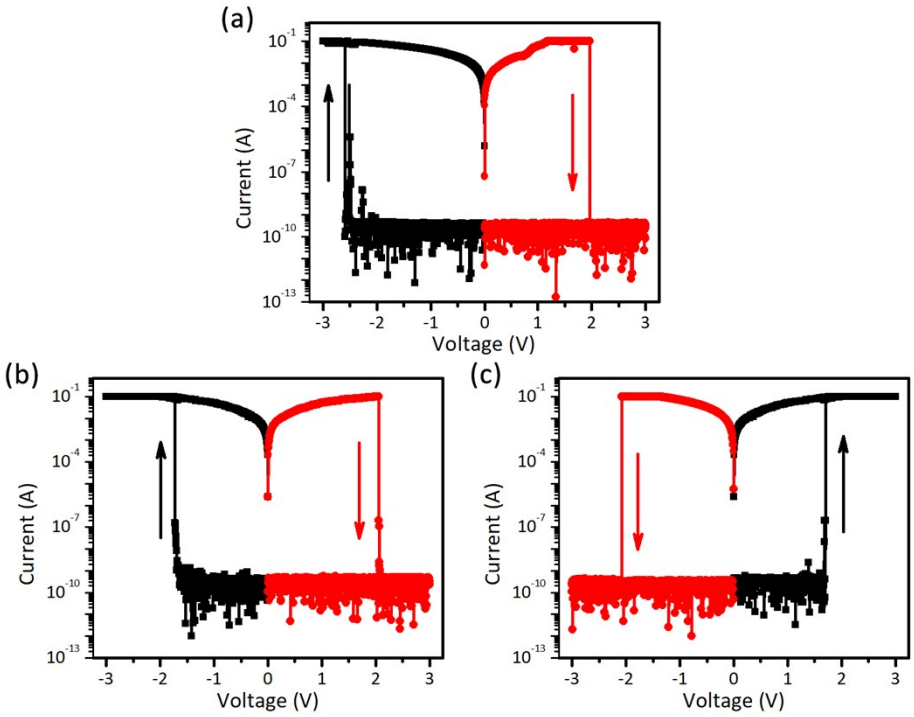

Fig. S7 (a) The I-V characteristics of Au/CPR1/ITO device. (b) and (c) The I-V characteristics of symmetric device Au/CPR1/Au. (The thickness of CPR1 film is 150 nm and the diameter of top electrode is 100 μm.)

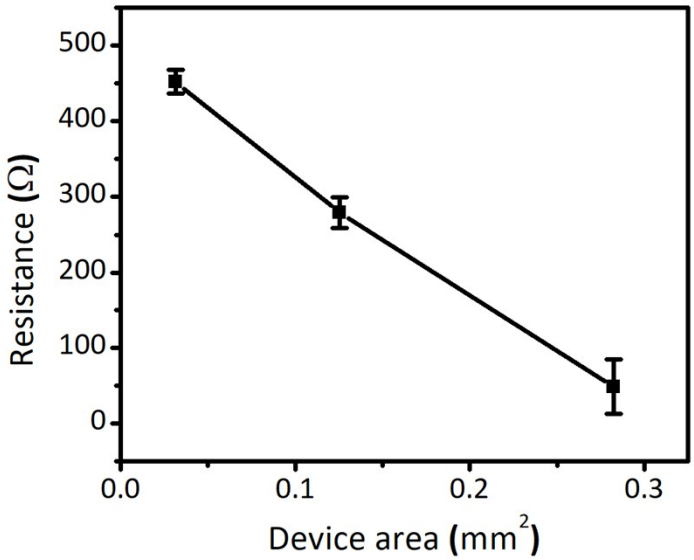

Fig. S8 Device area-dependence of LRS resistance for Al/CPR1/ITO. (The diameter of top electrode: 100, 200 and 300 μm,and the thickness of CPR1 film is 150 nm).

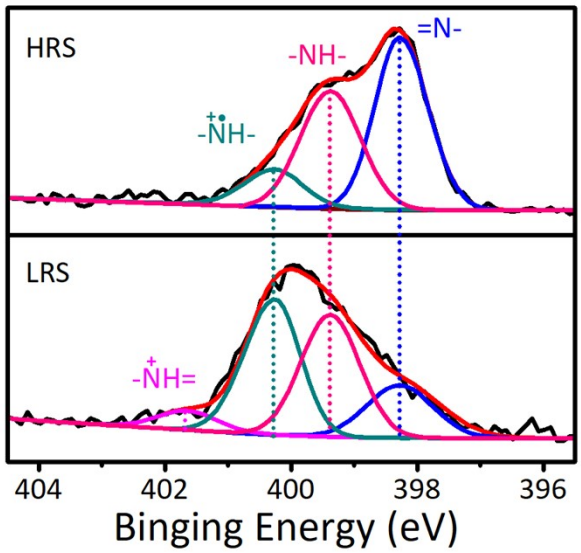

Fig. S9 N 1s XPS spectra of CPR1 device in HRS and LRS.

2.6 Flexibility of fully-printed CPR1 RRAM device arrays

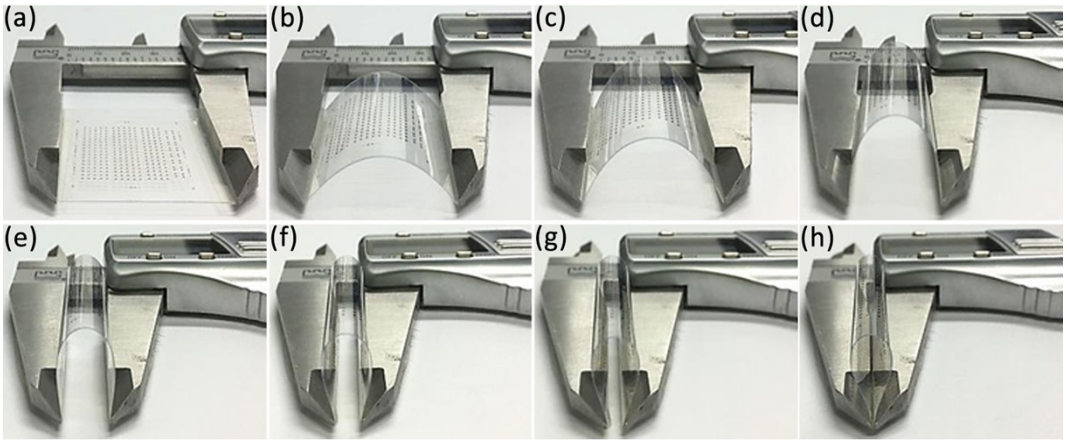

Fig. S10 The digital photos of flexible Au/CPR1/Au/PET device at different curvature radius: (a) flat, (b) 23 mm, (c) 16 mm, (d) 11 mm, (e) 6 mm, (f) 5 mm, (g) 4 mm, and (h) 3mm.

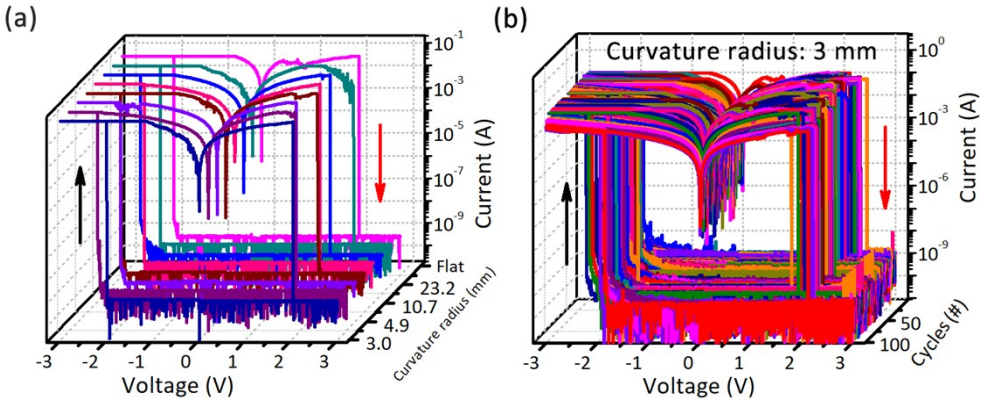

Fig. S11 The I-V characteristics of the flexible device (a)at different curvature radius and (b)after repeatedly bending different cycles at the curvature radius of 3 mm.

Table S3 The comparison of mechanical stability of the flexible RRAM devices fabricated by fully-printing or semi-printing process.

Storage medium (DT[a])	Electrode (DT)	Substrate	Flexibility				Ref.
			Radius[b] (mm)	Bending cycles	ON/OFF ratio	V_{set} (V)	
CPR1 (drop casting)	**Au (Coating)**	**PEN**	**3**	**1000**	**10^8**	**1.8**	**This work**
$SrTiO_3$-PVA (spray printing)	Ag (reverse offset printing)	PET	15	500	30	2.3	12
WSe_2 (aerosol jet printing)	Ag/CNT (aerosol jet printing)	Kapton paper	50	1	10^2	0.7	13
SoG (Spin coating)	PEDOT:PSS/Ag (inkjet printing)	PEN	15	1000	10^4	5.5	14
pEGDMA (CVD[c])	Ag (inkjet printing)	Paper	-	100	10^2	1	15
Parylene (CVD)	W/Al (lithography)	-	10	500	10^2	2.2	16
TiO_2 NP (inkject printing)	Carbon/Ag (screen printing/ Inkjet printing)	A4 paper	10	1000	10^3	2	17

[a] Deposition technique; [b] Minimum bending radius; [c] Chemical vapor deposition;

References

1 G. L. Yuan, N. Kuramoto and M. Takeishi, *Polym. Adv. Technol.*, 2003, **14**, 428-432.
2 B. Wang, J. He, D. Sun, R. Zhang, B. Han, Y. Huang and G. Yang, *Eur. Polym. J.*, 2005, **41**, 2483-2487.
3 G. Anitha and E. Subramanian, *J. Polym. Sci. A Polym. Chem.*, 2006, **44**, 281-294.
4 Y. Wang, X. Wang, J. Li, Z. Mo, X. Zhao, X. Jing and F. Wang, *Adv. Mater.*, 2001, **13**, 1582-1585.
5 A. Harada and M. Kamachi, *Macromolecules*, 1990, **23**, 2821-2823.
6 Y. Hasegawa, Y. Inoue, K. Deguchi, S. Ohki, M. Tansho, T. Shimizu and K. Yazawa, *J. Phys. Chem. B*, 2012, **116**, 1758-1764.
7 S. P. Park, Y. J. Tak, H. J. Kim, J. H. Lee, H. Yoo and H. J. Kim, *Adv. Mater.*, 2018, **30**, 1800722.1-1800722.8.
8 B. Chen, B. Gao, S. W. Sheng, L. F. Liu, X. Y. Liu, Y. S. Chen, Y. Wang, R. Q. Han, B. Yu and J. F. Kang, *IEEE Electron Device Lett.,* 2011, **32**, 282-284.
9 S. Gao, G. Liu, Q. Chen, W. Xue, H. Yang, J., Shang, B. Chen, F. Zeng, C. Song, F. Pan and R. W. Li, *ACS Appl. Mater. Interfaces*, 2018, **10**, 6453-6462.
10 B. Hu, X. Zhu, X. Chen, L. Pan, S. Peng, Y. Wu, J. Shang, G. Liu, Q. Yan and R. W. Li, *J. Am. Chem. Soc.*, 2012, **134**, 17408-17411.
11 Y. Q. Zhuo, Y. Jiang, R. Zhao, L. P. Shi, Y. Yang, T. C. Chong and J. Robertson, *IEEE Electron Device Lett.*, 2013, **34**, 1130-1132.
12 M. A. U. Khalid, S. W. Kim, J. Lee, A. M. Soomro, M. M. Rehman, B. G. Lee and K. H. Choi, *Polymer*, 2020, **189**, 122183.
13 Y. Li, M. Sivan, J. X. Niu, H. Veluri, E. Zamburg, J. Leong, U. Chand, S. Samanta, X. Wang, X. Feng, Y. Zhao and A. V. Y. Thean, *IEEE Sens. J.* 2020, **20**, 4653-4659.
14 B. Huber, P. B. Popp, M. Kaiser, A. Ruediger and C. Schindler, *Appl. Phys. Lett.*, 2017, **110**, 143503.
15 B. H. Lee, D. I. Lee, H. Bae, H. Seong, S. B. Jeon, M. L. Seol, J. W. Han, M. Meyyappan, S. G. Im and Y. K. Choi, *Sci. Rep.* 2016, **6**, 38389.
16 Y. Cai, J. Tan, L. YeFan, M. Lin and R. Huang, *Nanotechnology*, 2016, **27**, 275206.
17 D. H. Lien, Z. K. Kao, T. H. Huang, Y. C. Liao, S. C. Lee and J. H. He, *ACS Nano*, 2014, **8**, 7613-7619.